First-principles investigations on the mechanical, thermal, electronic, and optical properties of the defect perovskites Cs_2SnX_6 (X = Cl, Br, I)*

Hai-Ming Huang(黄海铭)[1,2], Zhen-Yi Jiang(姜振益)[1,†], and Shi-Jun Luo(罗时军)[2]

[1] *Shaanxi Key Laboratory for Theoretical Physics Frontiers, Institute of Model Physics, Northwest University, Xi'an* 710069, *China*

[2] *School of Science, Hubei University of Automotive Technology, Shiyan* 442002, *China*

(Received 29 March 2017; revised manuscript received 22 May 2017; published online 31 July 2017)

The mechanical properties, thermal properties, electronic structures, and optical properties of the defect perovskites Cs_2SnX_6 (X = Cl, Br, I) were investigated by first-principles calculation using PBE and HSE06 hybrid functional. The optic band gaps based on HSE06 are 3.83 eV for Cs_2SnCl_6, 2.36 eV for Cs_2SnBr_6, and 0.92 eV for Cs_2SnI_6, which agree with the experimental results. The Cs_2SnCl_6, Cs_2SnBr_6, and Cs_2SnI_6 are mechanically stable and they are all anisotropic and ductile in nature. Electronic structures calculations show that the conduction band consists mainly of hybridization between the halogen p orbitals and Sn 5s orbitals, whereas the valence band is composed of the halogen p orbitals. Optic properties indicate that these three compounds exhibit good optical absorption in the ultraviolet region, and the absorption spectra red shift with the increase in the number of halogen atoms. The defect perovskites are good candidates for probing the lead-free and high power conversion efficiency of solar cells.

Keywords: first-principles calculation, perovskites, elastic properties, optical properties

PACS: 63.20.dk, 71.20.–b, 87.19.rd, 78.40.Fy **DOI:** 10.1088/1674-1056/26/9/096301

1. Introduction

Perovskites compounds, especially pure inorganic and inorganic/organic halides, such as $CsSnI_3$, methyl ammonium lead iodide $CH_3NH_3PbI_3$, and formamidinium lead iodide $HC(NH_2)_2PbI_3$, have been proved to be some of the most promising materials in solar cells.[1–3] The ABX_3 type halide-based hybrid perovskites, where A is a metal atom or molecular cation, B is Sn or Pb, and X is a halide atom (Cl, Br, or I), are attracting an increasing amount of attention for applications due to advantageous optical properties and high power conversion efficiency.[4–10] Since Miyasaka *et al.*[11] pioneered the incorporation of the hybrid organic–inorganic perovskite halides $CH_3NH_3PbI_3$ into solar cells, the power conversion efficiency of this kind of solar cell increased from the begging of 3.8% to the current 20.1% in a few years.[12] However, the presence of toxic elements and instabilities of these perovskites halides greatly limit their widespread applications in efficient field-effect transistors light-emitting diodes, and photovoltaic devices.[13–17] Therefore, looking for non-toxic, environmentally friendly, and high conversion efficiency of new perovskite-type solar cell materials has become a current research hotspot.

Recently, Falaras *et al.*[18] reported three defect perovskites compounds Cs_2SnX_6 (X = Cl, Br, I). They found Cs_2SnCl_6, Cs_2SnBr_6, and Cs_2SnI_6 are all direct band gap semiconductors and can be used in dye-sensitized solar cells. They also found these three compounds are air-stable, and the dye-sensitized solar cells based on Cs_2SnI_6 hole-transporting materials present a power conversion efficiency of 4.23% at 1 sun illumination. Neilson *et al.*[19] pointed out that the greatest advantage of this kind of defect perovskites is that the Cs_2SnX_6 compounds contain Sn^{4+} rather than Sn^{2+} in the B-site, which makes it more stable under exposure to air and moisture. However, Xiao[20] and colleagues indicated the real valence state of Sn in Cs_2SnI_6 is +2 rather than +4. Although there are different opinions about the valence state of Sn cations in the defect perovskites compounds, it does not prevent the researchers from doing theoretical and experimental investigations on the new lead-free perovskite solar cell materials.[21–23]

The mechanical and thermal properties of perovskite are important for practical applications in solar cells. On the one hand, the absorption performances of perovskite solar cell strongly rely on the crystallinity and stress state of the perovskite layer.[24] On the other hand, as very important thermal parameters, the Debye temperature and melting temperature are related to the bond strength, which is important for the preparation of solar cell devices. Therefore, it is essential to study the mechanical and thermal properties of perovskite type solar cell materials. In this paper, we study the structural, mechanical, thermal, electronic and optical properties of the defect perovskites Cs_2SnX_6 (X = Cl, Br, I) by first-principles

*Project supported by the National Natural Science Foundation of China (Grant Nos. 51572219 and 11447030), the Natural Science Foundation of Shaanxi Province of China (Grant No. 2015JM1018), and Graduate's Innovation Fund of Northwest University of China (Grant No. YJG15007).

†Corresponding author. E-mail: jiangzy@nwu.edu.cn

© 2017 Chinese Physical Society and IOP Publishing Ltd

calculations. Our findings shed light on the key properties that are hard to measure experimentally and probing the lead-free solar cells materials.

2. Computational details

First-principles calculations were carried out to study various physical properties of the defect perovskites by using the Vienna *ab initio* simulation package (VASP).[25] Generalized gradient approximation (GGA) of Perdew–Burke–Ernzerh (PBE) was used to describe the exchange-correlation functional.[26] It is well known that PBE usually underestimates the band-gap, which will result in unreasonable optic properties. In order to overcome this predicament, band gap correction was considered by using range separated hybrid functional (HSE06),[27] which can give improved approximate results to match with experimental data. The electronic configurations: $6s^1$ for Cs, $5s^25p^2$ for Sn, $3s^23p^5$ for Cl, $4s^24p^5$ for Br, and $5s^25p^5$ for I were used in calculations. The plane wave cut-off energy was set to 450 eV. A mesh of $9\times9\times9$ k-points was used for calculating the electronic, mechanical, thermal, and optic properties. The convergence tolerances of the energy and the force are 1.0×10^{-6} eV and 1.0×10^{-2} eV/Å, respectively.

3. Results and discussion

3.1. Structural properties

Cs_2SnX_6 chemical composition presents the cubic anti-fluorite phase with the space group Fm-$3m$ in cubic structure as shown in Fig. 1. In this structure, the defect perovskites Cs_2SnX_6 own the same structure with K_2PtCl_6, in which the isolated $[SnX_6]^{2-}$ anions octahedra bridged by Cs^+ cations, the Sn^{4+} cations formed a face centered cubic lattice and are surrounded by an X_6 octahedral.[17,18,28] Firstly, a volume optimization process was carried out to predict the optimal structure. Calculated equilibrium lattice constants are summarized and compared with available theoretical and experimental data in Table 1.

One can observe that the optimized lattice constants of Cs_2SnCl_6 are almost the same as those of the experimental results. However, there is a slight deviation for Cs_2SnBr_6 and for Cs_2SnI_6, respectively. This slight deviation does not affect further research. On the whole, there is a good agreement between the optimized lattice constants and the experimental findings and available theoretical data. Furthermore, one can see that the lattice constants increase in the order from Cs_2SnCl_6 to Cs_2SnBr_6 to Cs_2SnI_6. The phenomenon is due mainly to the size differences between the univalent anion Cl^-, Br^-, and I^-.

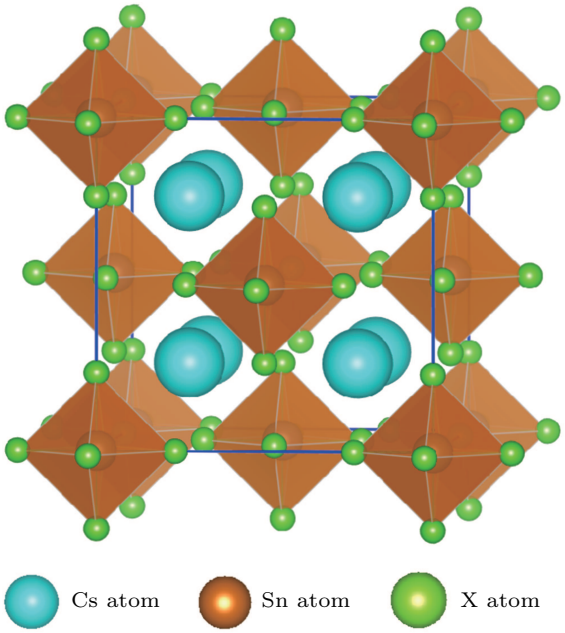


Fig. 1. (color online) Crystal structure of the defect perovskites Cs_2SnX_6 (X = Cl, Br, I). Thick blue lines represent the unit cell edges.

Table 1. Optimized lattice constants (Å) of Cs_2SnX_6 (X = Cl, Br, I). Experimental and other theoretical values are included.

Compounds	Cs_2SnCl_6	Cs_2SnBr_6	Cs_2SnI_6
Present	10.384	11.021	11.935
Experimental	10.382[a]	10.837[a]	11.638[a]
	10.3552[b]	10.770[c]	11.652[d]
			11.627[e]
Theoretical	10.846[a]	11.218[a]	12.016[a]
	10.724[f]	11.243[f]	12.032[f]

[a]Ref. [17]. [b]Ref. [28] [c]Ref. [29] [d]Ref. [30]. [e]Ref. [31]. [f]Ref. [32].

3.2. Mechanical properties

It is known that first-principles methods are often used to calculate reliable elastic properties of solid materials. The criterions for mechanical stability of cubic crystals are given by[33]

$$C_{11}>0, C_{11}-C_{12}>0, C_{11}+2C_{12}>0, C_{44}>0. \quad (1)$$

Table 2 summarizes the calculated elastic constants C_{ij} of the defect perovskites Cs_2SnX_6. One can see that the elastic constants satisfy these generalized stability criterions, indicating these three compounds are mechanically stable. Meanwhile, the elastic constant C_{11} decreases from chlorine to bromine to iodine in Cs_2SnX_6 (X = Cl, Br, I), meaning that the trend of resistance one-way compression declines. Cs_2SnCl_6 presents more strong resistance for one-way compression as compared to Cs_2SnBr_6 and Cs_2SnI_6. At the same time, the value of elastic constant C_{44} is less than that of C_{11}, which indicates that their resistance to pure shear deformation is weaker than that of the one-way compression.

Table 2. Calculated elastic properties C_{ij}, shear anisotropy factor A, bulk modulus B, shear modulus G, Pough's ratio B/G, Frantesvich ratio G/B, Young's modulus Y, Poisson's ratio υ, Kleinman parameter ξ, Debye temperature Θ_D, and melting temperature M_t for Cs_2SnX_6 (X = Cl, Br, I).

Properties	Cs_2SnCl_6	Cs_2SnBr_6	Cs_2SnI_6
C_{11}/GPa	36.1	22.0	14.4
C_{12}/GPa	17.6	11.5	7.0
C_{44}/GPa	15.0	10.1	6.0
Shear anisotropy factor A	1.62	1.92	1.62
Bulk modulus B/GPa	23.7	15	9.46
Shear modulus G/GPa	12.3	7.76	4.94
Pough's ratio B/G	1.92	1.93	1.92
Frantesvich ratio G/B	0.52	0.51	0.52
Young's modulus Y/GPa	31.5	19.8	12.6
Poisson's ratio υ	0.27	0.27	0.28
Kleinman parameter ξ	0.61	0.64	0.61
Debye temperature Θ_D/K	196	133	96.8
Melting temperature M_t/K	776±300	683±300	638±300

Using the elastic constants, some mechanical properties including shear anisotropy factor (A), bulk modulus (B), shear modulus (G), Pough's ratio (B/G), Frantesvich ratio (G/B), Young's modulus (Y), Poisson's ratio (υ) and Kleinman parameter (ξ) are also calculated and presented in Table 2. The shear anisotropy factor A is used to decide the anisotropic or isotropic characteristic of a solid. In general, the shear anisotropic factor for isotropic crystals is $A = 1$, while for anisotropic crystals it is $A \neq 1$. The shear anisotropic factors reported in Table 2 indicate Cs_2SnX_6 compounds are all anisotropic. It is clear that the level of anisotropy for Cs_2SnBr_6 is the highest among these three defect perovskites. Pough's ratio B/G and Frantesvich G/B ratio provide the brittleness or ductility of a compound. If $B/G < 1.75$ ($G/B > 0.571$), the material is brittle, otherwise, the ductile behavior is predicted.[34] Present values of Pough's ratio for Cs_2SnCl_6, Cs_2SnBr_6 and Cs_2SnI_6 are bigger than 1.75, therefore these defect perovskites are ductile in nature.

Young's modulus Y is an important parameter in showing the stiffness of a solid material. The larger the Young's modulus, the stiffer the solid material will be. From Table 2, it is clear that the Young's modulus decreases with large anion size, indicting Cs_2SnCl_6 is stiffer than Cs_2SnBr_6 and Cs_2SnI_6, and the capability of resisting elastic deformation decreases from Cs_2SnCl_6 to Cs_2SnBr_6 to Cs_2SnI_6. Poisson's ratio υ gives some informations about the character of force acting on solid materials. The forces among the atoms constituting the material are central if the value of υ lies between 0.25 and 0.50. The obtained Poisson ratio υ for Cs_2SnCl_6, Cs_2SnBr_6 and Cs_2SnI_6 are just in this range which means that interatomic forces in Cs_2SnX_6 are central.

3.3. Thermal properties

Debye temperature Θ_D is a fundamental parameter for materials' thermodynamic properties, and it is closely related to specific heat, bond strength, elastic constants, and melting temperature.[35] Θ_D can be predicted by the average sound velocity V_m according to[33,36]

$$\Theta_D = V_m \frac{h}{k}\left[\frac{3n}{4\pi}\left(\frac{N_A\rho}{M}\right)\right]^{1/3}, \tag{2}$$

where h represents Plank's constant, k is the Boltzman constant, n is the number of atoms per molecule, N_A is the Avogadro number, ρ is the density of the solid, and M represents the molecular weight. The average sound velocity V_m was calculated by[33,36]

$$V_m = \left[\frac{1}{3}\left(\frac{2}{v_t^3} + \frac{1}{v_l^3}\right)\right]^{-(1/3)}, \tag{3}$$

where v_t and v_l are the transverse and longitudinal sound velocity, respectively, which is calculated by[37]

$$v_l = \sqrt{\frac{3B+4G}{3\rho}}, \tag{4}$$

$$v_t = \sqrt{\frac{G}{\rho}}. \tag{5}$$

The calculated Debye temperatures of Cs_2SnX_6 (X = Cl, Br, I) are also listed in Table 2. Obviously, the values of Debye temperature Θ_D decrease in the following sequence: Cs_2SnCl_6 >Cs_2SnBr_6 >Cs_2SnI_6. The Cs_2SnCl_6 presents the highest Debye temperature indicating the higher melting temperature. At present, there are no theoretical calculations as well as experimental measurements reported on the Debye temperature for Cs_2SnCl_6 and Cs_2SnBr_6. However, there is a large deviation for the Debye temperature of Cs_2SnI_6 between the present work 96.8 K and experimental result 149 K obtained by heat capacity data.[18] The main reason is the difference of lattice constant between theoretical calculations and experimental measurement. In general, the lattice constant has an important influence on the calculation of Debye temperature. As a comparison, we use the experimental lattice constant of 11.6527 Å[22] to calculate the Debye temperature of Cs_2SnI_6; the obtained value of Θ_D = 141.2 K is very close to the experimental results.

The Deby temperature corresponds to the highest frequency of the lattice vibration, which is actually a reflection of the strongest bonding of the crystal. Recently, Kumar *et al.*[38] obtained a linear relation between Deby temperature and melting temperature for II–VI and III–V semiconductors. In general, for the same compound, a larger Debye temperature means a higher melting temperature.[39] The melting temperature M_t of Cs_2SnX_6 can be calculated by elastic constants C_{11} according to the following expression:[33,40]

$$M_t = \left[553\ \text{K} + \left(\frac{5.91\ \text{K}}{\text{GPa}}\right)C_{11}\right] \pm 300\ \text{K}. \tag{6}$$

Calculated melting temperatures are also shown in Table 2. It is clear that the melting temperature of Cs_2SnCl_6 is higher than that of Cs_2SnCl_6 and Cs_2SnBr_6. The results are in agreement with the results of Debye temperature.

3.4. Electronic properties

Density of states and band structures calculations predict the direct band gaps at the Γ point for Cs_2SnCl_6, Cs_2SnBr_6 and Cs_2SnI_6. The results are consistent with the ones of other investigators.[18,22] Band gap values, as obtained by PBE and HSE06 using the optimized lattice constants, are listed in Table 3. Obviously, the HSE06 results are a lot closer to the experimental measurements as compared to the PBE ones. The band structure of Cs_2SnCl_6 indicates a band gap of 3.83 eV, which consists with the experimentally measured optical gap of 3.9 eV and is better than other theoretical calculations. For the Cs_2SnBr_6 and Cs_2SnI_6, the direct band gaps are 2.36 and 0.92 eV, respectively, which is lower than the experimentally measured optical gap. There are two main reasons for this discrepancy: one is the difference of lattice constants between theoretical calculations and experimentally measured ones, the other arises from the fact that first-principles calculations often underestimate the band gap.

Table 3. Calculated band gap (eV) of Cs_2SnX_6 (X = Cl, Br, I) using the PBE and HSE06 functional. Experimental and other theoretical values are also included.

Compounds	Cs_2SnCl_6	Cs_2SnBr_6	Cs_2SnI_6
Present (PBE)	2.27	1.51	0.36
Present (HSE06)	3.83	2.36	0.92
Experimental	3.9[a]	2.7[a]	1.26[a]
Experimental			1.25[b]
Theoretical (PBE)	2.228[a]	1.476[a]	0.346[a]
Theoretical (GW0)	3.226[a]	2.241[a]	0.883[a]
Theoretical (HSE06)			0.97[b]

[a]Ref. [18]. [b]Ref. [22].

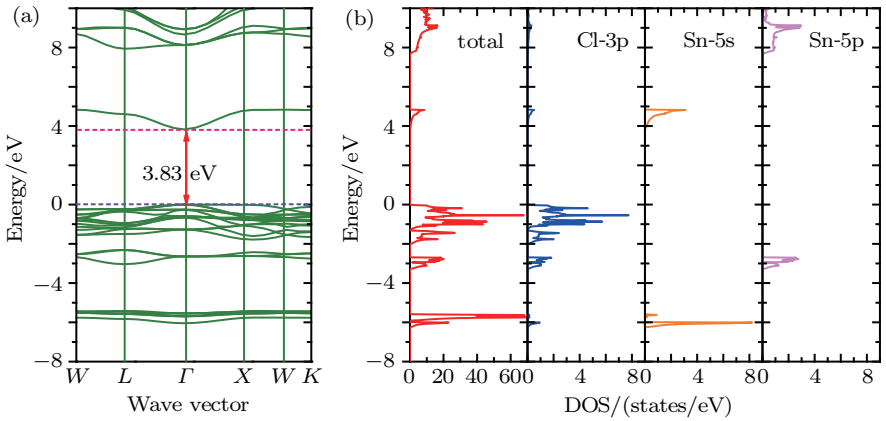


Fig. 2. (color online) (a) Band structures, (b) total and orbital-projected densities of states for Cs_2SnCl_6 based on the HSE06.

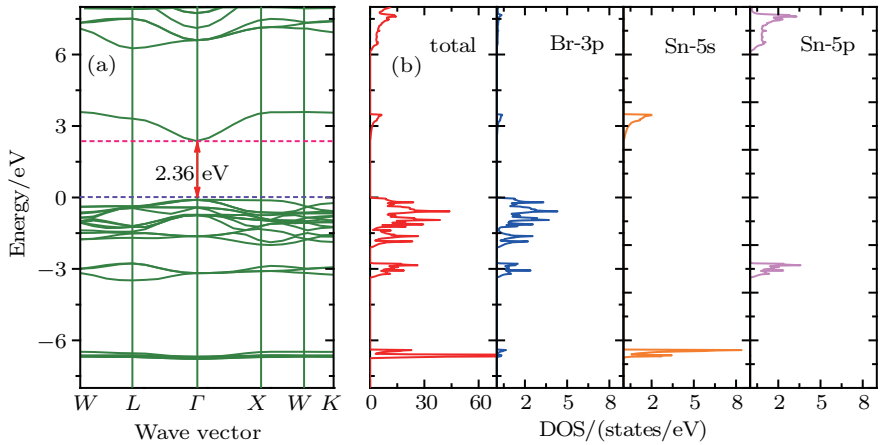


Fig. 3. (color online) (a) Band structures, (b) total and orbital-projected densities of states for Cs_2SnBr_6 based on the HSE06.

Figures 2–4 present the band structures, total and orbital-projected densities of states (DOSs) for title compounds based on the HSE06. We have not plotted the projected DOS of Cesium since its negligible contribution to the total DOS. It is clear that these three compounds have very similar electronic structures as well as a delicate difference. The orbital-

projected DOSs indicate that the conduction band near the Fermi level is mainly composed of halogen p orbitals hybridized with Sn 5s orbitals, and the upper conduction bands, starting from 7.66, 6.12 and 4.38 eV for Cs_2SnCl_6, Cs_2SnBr_6 and Cs_2SnI_6, respectively. There is a forbidden gap of 2.86 eV for Cs_2SnCl_6, 2.85 eV for Cs_2SnBr_6 and 2.36 eV for Cs_2SnI_6 between the two conduction bands. On the other hand, the valence band is constituted of the halogen p orbitals, and their band widths are 1.99 eV for Cs_2SnCl_6, 2.08 eV for Cs_2SnBr_6 and 2.22 eV for Cs_2SnI_6, respectively. Another halogen p orbital presents hybridization with Sn 5p orbital between −3.40 to −2.75 eV. In a deeper band, from −5.91 eV to −5.59 eV for Cs_2SnCl_6, from −6.73 eV to −6.39 eV for Cs_2SnBr_6 and from −6.95 eV to −6.67 eV for Cs_2SnI_6, the valence band is mainly made of the Sn 5s orbital.

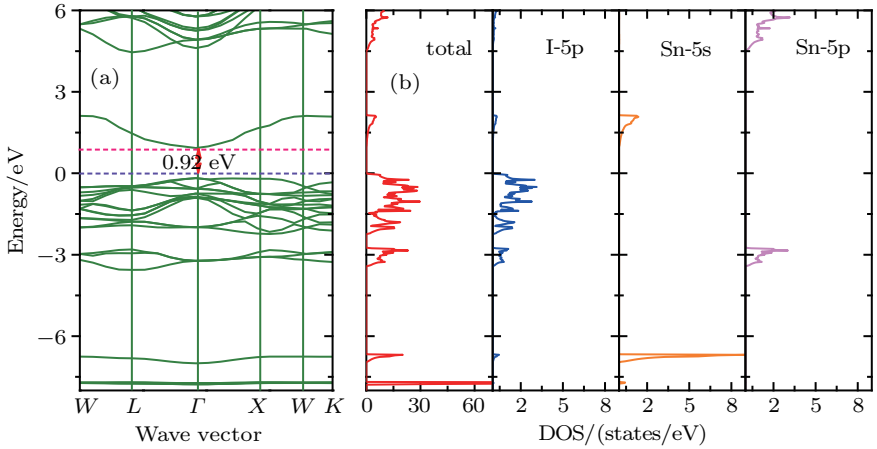


Fig. 4. (color online) (a) Band structures, (b) total and orbital-projected densities of states for Cs_2SnI_6 based on the HSE06.

3.5. Optic properties

The optical properties of a semiconductor material are closely related to their electronic band structures; it is usually obtained from the dielectric function by the formula that is given by[41,42]

$$\varepsilon(\omega) = \varepsilon_1(\omega) + i\varepsilon_2(\omega), \tag{7}$$

where ω is the angular frequency, and $\varepsilon_1(\omega)$ and $\varepsilon_2(\omega)$ are the real and the imaginary parts of the complex dielectric function, respectively.

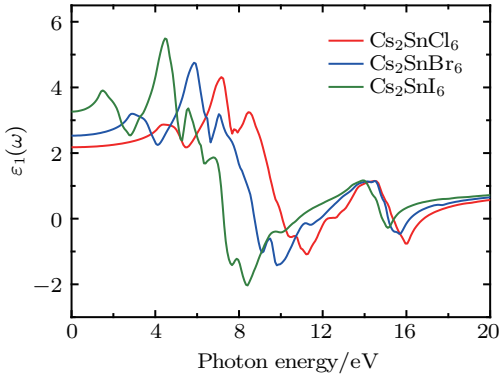


Fig. 5. (color online) Real part of the dielectric function for the defect perovskites Cs_2SnX_6 (X = Cl, Br, I).

The dielectric functions of Cs_2SnCl_6, Cs_2SnBr_6, and Cs_2SnI_6 with changes in photon energy were calculated up to 20.0 eV and shown in Figs. 5 and 6. The static dielectric constants $\varepsilon_0(\omega)$ are 2.17 for Cs_2SnCl_6, 2.53 for Cs_2SnBr_6, and 3.26 for Cs_2SnI_6 and the values increase with increasing halogen atomic number. The real part $\varepsilon_1(\omega)$ is positive up to 10.1 eV, 8.70 eV, and 7.23 eV for Cs_2SnCl_6, Cs_2SnBr_6, and Cs_2SnI_6, respectively. In this area, for Cs_2SnI_6, the real part has three peaks located at 4.39, 7.15, and 8.45 eV. For Cs_2SnBr_6, it presents several peaks at 2.92, 5.93, and 7.03 eV. Also for Cs_2SnI_6, its three peaks are located at 1.48, 4.46, and 5.58 eV.

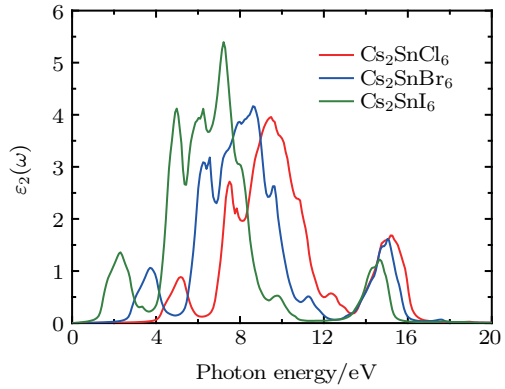


Fig. 6. (color online) Imaginary part of the dielectric function for the defect perovskites Cs_2SnX_6 (X = Cl, Br, I).

The imaginary dielectric function $\varepsilon_2(\omega)$ gives some important information on the multifarious interband transitions between the valence and conduction bands. The imaginary part for Cs_2SnCl_6 exhibits five major absorption peaks at 3.80,

5.19, 7.50, 9.49, and 15.23 eV. The five major absorption peaks of Cs_2SnBr_6 are located at 2.32, 3.74, 6.54, 8.65, and 15.05 eV. The five major absorption peaks of Cs_2SnI_6 are located at 0.90, 2.30, 4.98, 7.26, and 14.63 eV. These peaks are associated with the transition from valence bands to conduction ones. The lower energy peaks are relative to the electronic transition between the Cl-3p, Br-4p, and I-5p states in the upper valence bands and the Sn-5s states in conduction bands.

In addition to the real and imaginary components of the dielectric functions, the refractive index $n(\omega)$, extinction coefficient $k(\omega)$, absorption coefficient $\alpha(\omega)$, reflectivity coefficient $R(\omega)$, optical conductivity $\kappa(\omega)$ and energy loss function $L(\omega)$ are calculated and plotted in Fig. 7. Refractive index is an indispensable parameter to describe the optical properties of materials and has an important impact on optic devices such as solar cell and detectors.[43] From Fig. 7(a), the curves of the refractivity index of Cs_2SnCl_6, Cs_2SnBr_6 and Cs_2SnI_6 coincide with the real part of the dielectric functions. The static refractive index $n(0)$ for low frequency at 0 eV and their peak values are presented in Table 4. It is clear that the $n(0)$ and peak values increase with the increasing of the size of halogen anions. Extinction coefficient $k(\omega)$ describes the attenuation of an electromagnetic wave in a material. In the low energy infrared region in Fig. 7(b), the value of the extinction coefficient is close to zero, which indicates these three defect perovskites are transmitted to the infrared spectrum.

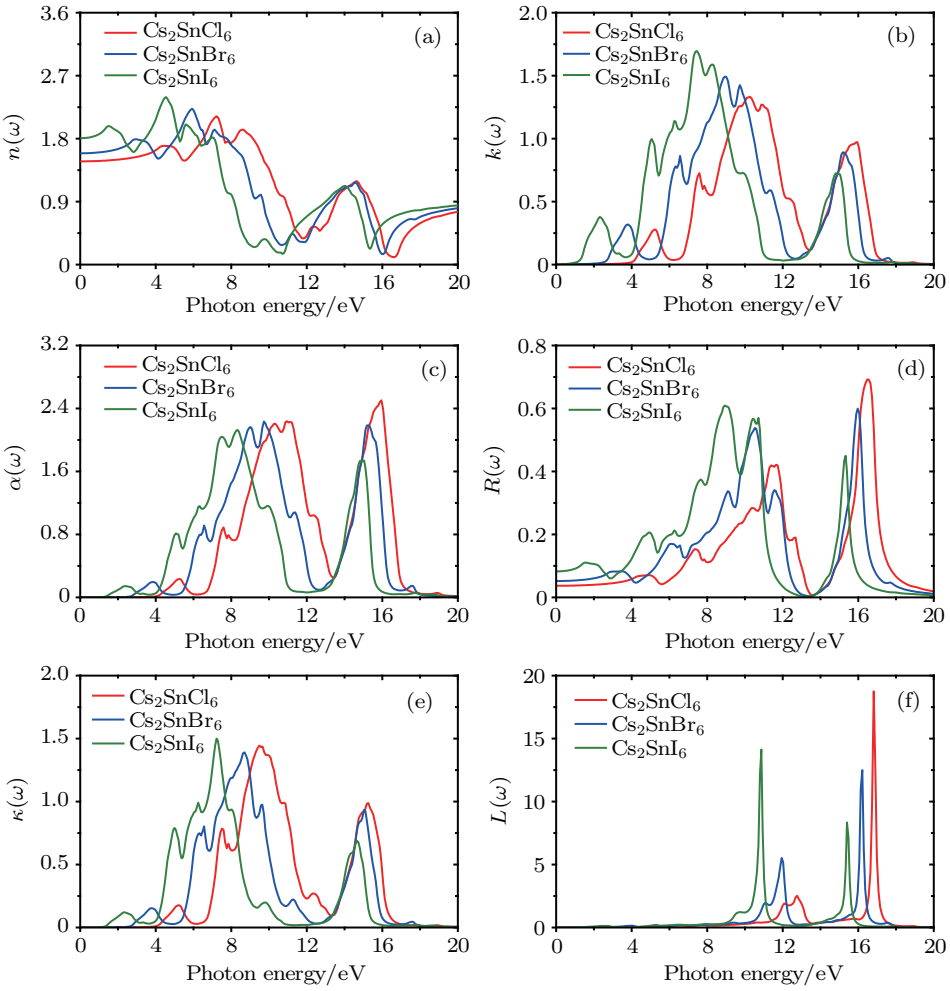


Fig. 7. (color online) Refractive index $n(\omega)$, extinction coefficient $k(\omega)$, absorption coefficient $\alpha(\omega)$, reflectivity coefficient $R(\omega)$, optical conductivity $\kappa(\omega)$ and energy loss function $L(\omega)$ of the defect perovskites Cs_2SnX_6 (X = Cl, Br, I).

Table 4. Static refractive index, static reflectivity, maximum refractive index and maximum reflectivity for Cs_2SnX_6 (X = Cl, Br, I).

Compounds	Refractivity index		Reflectivity	
	$n(0)$	maximum	$R(0)$	maximum
Cs_2SnCl_6	1.47	2.12	0.03	0.69
Cs_2SnBr_6	1.59	2.23	0.05	0.60
Cs_2SnI_6	1.81	2.39	0.08	0.61

The absorption coefficient can be further calculated according to the refractive index and extinction coefficient. From Fig. 7(c), one can see that the absorption edges are located at 3.96, 2.52, and 1.07 eV for Cs_2SnCl_6, Cs_2SnBr_6, and Cs_2SnI_6, respectively. These absorption edge values are near the corresponding band gaps as predicted by the HSE06 method. The absorption spectrum of the intrinsic defect perovskites Cs_2SnX_2 is mainly concentrated in the ultraviolet region. With

the increase of the number of halogen atoms, the absorption spectra have an obvious red shift, which means the Cs_2SnI_2 is a promising material for photoelectric conversion. Moreover, there are five obvious characteristic peaks in the absorption spectrum. The positions of the peaks and the absorption edges are all presented in Table 5. Obviously, the position moves towards a low energy area with the increasing size of the halogen ions, and the strongest peak is located at 15.9 eV for Cs_2SnCl_6, 9.73 eV for Cs_2SnBr_6, and 8.29 eV for Cs_2SnI_6, respectively. In the low energy range, the absorption coefficient is close to zero, indicating that its absorption of light waves in the low energy range is not obvious.

The static reflectivity $R(0)$ and the maximum reflectivity of the title compounds are listed in Table 4. Figure 7(d) depicts the curves of reflectivity as a functional of photon energy. It is clear that the zero frequency reflectivity increases in the following sequence: Cs_2SnCl_6<Cs_2SnBr_6<Cs_2SnI_6. The reflectivity for these three compounds in the infrared region is lower than 8.0% reflecting the case that the effect of surface reflection and internal grain boundary reflection on the low energy infrared wave band is small. The wavelength of the maximum reflectivity is obtained around 74.95 nm for Cs_2SnCl_6, 77.69 nm for Cs_2SnBr_6, and 138.9 nm for Cs_2SnI_6, respectively.

Table 5. The positions (eV) of the characteristic peaks and the absorption edges in the absorption spectrum for Cs_2SnX_6 (X = Cl, Br, I).

Compounds	Edge	Peak1	Peak2	Peak3	Peak4	Peak5
Cs_2SnCl_6	3.96	5.26	7.62	10.3	11.1	15.9
Cs_2SnBr_6	2.52	3.85	6.59	9.01	9.73	15.3
Cs_2SnI_6	1.07	2.40	5.10	7.46	8.29	15.0

The optical conductivity, which is decided by refractive index and absorption coefficient, is usually used to investigate the optical response of material. From Fig. 7(e), one can see that the optical conductivity follows the same trend as that of the absorption coefficient with increasing phonon energy. The optical conductivity of Cs_2SnCl_6 is zero when the phonon energy is smaller than 3.96 eV and bigger than 17.59 eV. For Cs_2SnBr_6, the optical conductivity is zero when the phonon energy is smaller than 2.52 eV and bigger than 18.10 eV. Also for Cs_2SnI_6, the optical conductivity is zero when the phonon energy is smaller than 1.07 eV and bigger than 19.87 eV. The maximum optical conductivity appears when the energy is 9.51, 8.71, and 7.24 eV for Cs_2SnCl_6, Cs_2SnBr_6, and Cs_2SnI_6, respectively.

The energy loss function is an important parameter in describing the energy loss when electrons pass through a dielectric. The function is directly relative to the real and imaginary components of dielectric functions, and the peak of the loss function is associated with plasma oscillation. Figure 7(f) depicts the energy loss function as a function of photon energy. One can see that the energy loss in two regions is very large, and the maximum energy loss points are located at 16.85, 16.23, and 10.85 eV for Cs_2SnCl_6, Cs_2SnBr_6, and Cs_2SnI_6u, respectively. The electronic energy loss for these three compounds is close to zero when the energy is bigger than 20.0 eV.

4. Conclusion

Employing the first-principles method within the PBE and HSE06 functional, we carried out a comprehensive study on the structural, mechanical, thermal, electronic, and optical properties of the defect perovskites Cs_2SnCl_6, Cs_2SnBr_6, and Cs_2SnI_6. The results indicate that the optimized lattice parameters are in good agreement with the available theoretical and experimental data. These three compounds are mechanically stable and they are all anisotropic and ductile in nature. Calculated Debye temperature and melting temperature decrease from Cs_2SnCl_6 to Cs_2SnBr_6 to Cs_2SnI_6. Density of states and band structures indicate direct band gaps for all the defect perovskites Cs_2SnX_6, which accords with other theoretical investigations. Orbital-projected DOSs indicate that the contribution to the conduction band mainly originates from the halogen p orbitals hybridized with Sn 5s orbitals, whereas the contribution to the valence band is consisted of the halogen p orbitals. Some parameters, which are closely related to optical properties such as dielectric functions, refractive index, extinction coefficient, absorption coefficient, reflectivity coefficient, optical conductivity, and energy loss function, are studied theoretically for the first time. The results indicate that these three materials exhibit good optical absorption in the ultraviolet region, and the absorption spectra red shift with the increase of the number of halogen atoms. In conclusion, these three defect perovskites are good candidates for probing the lead-free and high-power conversion efficiency of solar cells materials owing to their stable mechanical properties and excellent optical absorption in the ultraviolet region.

References

[1] Chung I, Lee B, He J, Chang R P H and Kanatzidis M G 2012 *Nature* **485** 486
[2] Baikie T, Fang Y, Kadro J M, Schreyer M, Wei F, Mhaisalkar S G, Graetzeld M and Whitec T J 2013 *J. Mater. Chem. A* **1** 5628
[3] Zhou H, Chen Q, Li G, Luo S, Song T B, Duan H S, Hong Z, You J, Liu Y and Yang Y 2014 *Science* **345** 542
[4] Brivio F, Walker A B and Walsh A 2013 *APL Mater.* **1** 042111
[5] Eperon G E, Paternò G M, Sutton R J, Zampetti A, Haghighirad A A, Cacialli F and Snaith H J 2015 *J. Mater. Chem. A* **3** 19688
[6] Weller M T, Weber O J, Henry P F, Di Pumpo A M and Hansen T C 2015 *Chem. Commun.* **51** 4180
[7] Lee C, Hong J, Stroppa A, Whangbo M H and Shim J H 2015 *RSC Adv.* **5** 78701
[8] Feng J and Xiao B 2014 *J. Phys. Chem. C* **118** 19655
[9] Yuan Y, Xu R, Xu H T, Hong F, Xu F and Wang L J 2015 *Chin. Phys. B* **24** 116302
[10] Du H J, Wang W C and Zhu J Z 2016 *Chin. Phys. B* **25** 108803
[11] Kojima A, Teshima K, Shirai Y and Miyasaka T 2009 *J. Am. Chem. Soc.* **131** 6050

[12] Boix P P, Agarwala S, Koh T M, Mathews N and Mhaisalkar S G 2015 *J. Phys. Chem. Lett.* **6** 898

[13] Lora da Silva E, Skelton J M, Parker S C and Walsh A 2015 *Phys. Rev. B* **91** 144107

[14] Szafranski M and Katrusiak A 2016 *J. Phys. Chem. Lett.* **7** 3458

[15] Yi H T, Wu X X, Zhu X Y and Podzorov V 2016 *Adv. Mater.* **28** 6509

[16] Chen Z, Wang J J, Ren Y, Yu C and Shum K 2012 *Appl. Phys. Lett.* **101** 093901

[17] Qiu X F, Cao B Q, Yuan S, Chen X F, Qiu Z W, Jiang Y N, Ye Q, Wang H Q, Zeng H B, Liu J and Kanatzidis M G 2017 *Sol. Energy Mater. Sol. Cells* **159** 227

[18] Kaltzoglou A, Antoniadou M, Kontos A G, Stoumpos C C, Perganti D, Siranidi E, Raptis V, Trohidou K N, Psycharis V, Kanatzidis M G and Falaras P 2016 *J. Phys. Chem. C* **120** 11777

[19] Maughan A E, Ganose A M, Bordelon M M, Miller E M, Scanlon D O and Neilson J R 2016 *J. Am. Chem. Soc.* **138** 8453

[20] Xiao Z W, Lei H C, Zhang X, Zhou Y Y, Hosono H and Kamiya T 2015 *Bull. Chem. Soc. Jpn.* **88** 1250

[21] Lee B, Stoumpos C C, Zhou N J, Hao F, Malliakas C, Yeh C Y, Marks T J, Kanatzidis M G and Chang R P H 2014 *J. Am. Chem. Soc.* **136** 15379

[22] Xiao Z W, Zhou Y Y, Hosono H and Kamiya T 2015 *Phys. Chem. Chem. Phys.* **17** 18900

[23] Saparov B, Sun J P, Meng W W, Xiao Z W, Duan H S, Gunawan O, Shin D, Hill I G, Yan Y F and Mitzi D B 2016 *Chem. Mater.* **28** 2315

[24] Feng J 2014 *APL Mater.* **2** 081801

[25] Kresse G and Furthmuller J 1996 *Comput. Mater. Sci.* **6** 15

[26] Perdew J P, Burke K and Ernzerhof M 1996 *Phys. Rev. Lett.* **77** 3865

[27] Heyd J, Scuseria G E and Ernzerhof M 2006 *J. Chem. Phys.* **124** 219906

[28] Torres D T, Freire J D and Katiyar R S 1997 *Phys. Rev. B* **56** 7763

[29] Brill T B, Gerhart R C and Welsh W A 1974 *J. Magn. Reson.* **13** 27

[30] Ketelaar J A A, Rietdijk A A and van Staveren C H 2010 *Recl. Trav. Chim. Pays-Bas* **56** 907

[31] Stoumpos C C, Malliakas C D and Kanatzidis M G 2013 *Inorg. Chem.* **52** 9019

[32] Wang G T, Wang D Y and Shi X B 2015 *AIP Advances* **5** 127224

[33] Gu J B, Wang C J, Zhang W X, Sun Bin, Liu G Q, Liu D D and Yang X D 2016 *Chin. Phys. B* **25** 126103

[34] Pugh S F 1954 *Philos. Mag.* **45** 823

[35] Duan Y H, Sun Y, Peng M J and Zhou S G 2014 *J. Alloy. Compd.* **585** 587

[36] Anderson O L 1963 *J. Phys. Chem. Solids* **24** 909

[37] Mujica A and Needs R J 1996 *J. Phys.: Conden. Matter* **8** L237

[38] Kumar V, Jha V and Shrivastava A K 2010 *Cryst. Res. Technol.* **45** 920

[39] Lu W F, Li C J, Sarac B, Şopu D, Yi J H, Tan J, Stoica M and Eckert J 2017 *J. Alloy. Compd.* **705** 445

[40] Fine M E, Brown M D and Marcus H L 1984 *Scr. Metall.* **18** 951

[41] Parvin R, Parvin F, Ali M S and Islam A K M A 2016 *Chin. Phys. B* **25** 083101

[42] Fahad S, Murtaza G, Ouahrani T, Khenata R, Yousaf M, Omran S B and Mohammad S 2015 *J. Alloy. Compd.* **646** 211

[43] Zhao S, Lan C, Ma J, Pandey S S, Hayase S and Ma T 2015 *Solid State Commun.* **213-214** 19